ELSEVIER

15 July 1998

OPTICS COMMUNICATIONS

Optics Communications 153 (1998) 134–152

Full length article

Twisted-nematic liquid-crystal pixelated active lens

Vincent Laude [1]

Thomson-CSF, Laboratoire Central de Recherches, Domaine de Corbeville, F-91404 Orsay Cedex, France

Received 18 July 1997; revised 26 January 1998; accepted 5 March 1998

Abstract

Liquid-crystal active lenses are classical imaging systems in which a liquid-crystal spatial light modulator is placed in a pupil plane. The modulator controls the phase of the optical wave in the pupil and achieves an arbitrary wavefront shape, that is limited only by the available modulation depth and resolution. The possibility of using a twisted-nematic liquid-crystal television in the pupil plane is investigated both experimentally and theoretically. The precise evaluation of the modulation characteristics is first discussed. Experimental results obtained both with monochromatic and polychromatic light illustrate the different sampling, quantization and chromatism effects discussed theoretically. Useful models for the computation of the point spread function and the modulation transfer function of a generic pixelated liquid-crystal active imaging system are presented for both in-focus and out-of-focus systems, and their numerical implementation is discussed.

1. Introduction

It is well known that the imaging characteristics of an optical system can be adequately described by the optical transfer function (OTF) in a pupil plane, or equivalently by the point spread function (PSF) which is simply related to the Fourier transform of the OTF [1]. In a classical optical imaging system using fixed elements like lenses, prisms and mirrors, the OTF and the PSF are fixed functions. For some applications it would be interesting to be able to modify at will the OTF, at least in the vicinity of an operating point. One interesting solution is to add a phase spatial light modulator (SLM) in the pupil plane of the optical imaging system (Fig. 1). Takaki et al. [2–4] have proposed and demonstrated experimentally such an active lens system. They used a phase-only liquid-crystal SLM (LC-SLM) attached to a thin lens, and demonstrated several different programmable functions, including image shifting and focus control. This concept is also closely related to programmable diffractive functions written onto SLMs [5–9,2–4]. If a constant phase pattern is written onto the SLM, the image forming characteristics will not be altered. However if the phase pattern represents a prism, the image will be shifted transversally which is equivalent to beam steering [10,11], whereas if it represents a thin lens the image will be translated longitudinally, or defocused [12–16]. Other image forming modifications controlled by certain phase patterns can be imagined as well. It can be noted that active imaging systems are also closely connected to applications such as aberration compensation and adaptive optics using liquid-crystals [17–20].

There exist several possibilities for the phase SLM, among which the liquid-crystal technology is the most widespread at the moment. Pure-phase modulation can be obtained in the optical birefringence mode using nematic liquid-crystals, which assume that the molecular directors are parallel throughout the liquid-crystal cell depth [21]. However, commercial liquid-crystal televisions (LCTVs) that are designed for display applications usually employ twisted-nematic liquid-crystals, but when employed as LC-SLM can hopefully provide for an approximate pure-phase modulation under certain experimental

[1] E-mail: laude@thomson-lcr.fr

0030-4018/98/$19.00
PII S0030-4018(98)00143-6

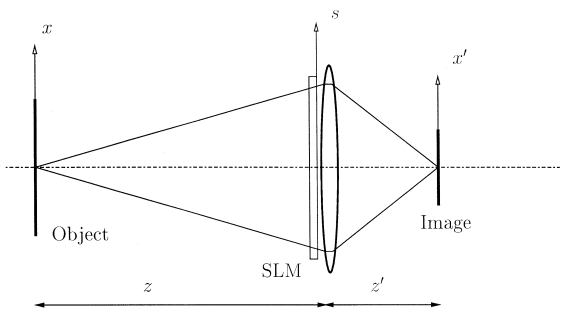

Fig. 1. Principle of the liquid-crystal active lens.

arrangements [22,8,9]. It is the purpose of this paper to study both experimentally and theoretically the use of a twisted-nematic LC-SLM in an active lens.

Section 2 presents a simplified but generic model of a liquid-crystal active lens, including the important issues of sampling and quantization. The material in this section is a collection of different results from the field of diffractive optics, but is presented here in the context of active lenses. Section 3 describes our procedure for precisely determining the amplitude and phase modulation of a twisted-nematic LCTV. The approach combines two previously proposed methods and couples them with a robust estimation algorithm. The problem of the determination of the amplitude and phase modulation of LC-SLMs has been the subject of a quite large number of papers in the last years, a situation that outlines the practical importance of these devices for optical information processing and also the importance of the correct determination of their modulation capabilities. Section 4 reports on experiments demonstrating image shifting and focus control for monochromatic illumination, and compares these results with the theoretical predictions regarding sampling and quantization. Chromatism is considered in Section 5, where white-light illumination is used, and the influence of the spectral bandwidth is discussed and illustrated experimentally. In Section 6, useful formulas are provided for computing the point spread function (PSF) and the modulation transfer function (MTF) for both in-focus and out-of-focus systems. Numerical simulations are compared with the experimental results.

2. Background

2.1. Sampling considerations

A generic liquid-crystal active imaging system is sketched in Fig. 1. The imaging system is represented by an equivalent thin lens, and the liquid-crystal spatial light modulator is assumed to be placed in the plane of the thin lens, defining the pupil plane. Obviously, a practical imaging system includes several lenses, that are moreover not necessarily thin, and the SLM cannot be physically present in exactly the same plane as a lens. However, if it can be assumed that the imaging system is perfectly corrected from aberrations for both the image and the intermediate pupil plane in which the SLM is actually placed, then within the Fresnel-Kirchoff approximation of diffraction [23] used here, the general case is essentially equivalent to the single thin lens case discussed here.

In the case of an out of focus optical system, the following convention is used following Goodman [1]: the image focus distance is measured in units of z' by $(1-\epsilon)z'$, e.g. $\epsilon = 0.3$ for 30% defocus, or $\epsilon = -0.3$ for -30% defocus. The coherent point spread function takes the form of a Fresnel transform [1]

$$P(x') = \int \exp\left(\frac{i\pi s^2 \epsilon}{\lambda z'(1-\epsilon)}\right) \exp\left(-2i\pi \frac{sx'}{\lambda z'(1-\epsilon)}\right) f(s)\,\mathrm{d}s. \tag{1}$$

For a perfectly focused imaging system ($\epsilon = 0$) the coherent point spread function simplifies to a Fourier transform of the pupil function, as is well known. Throughout the paper one-dimension notations will be used, since generalization to two-dimensions is straightforward.

A common feature of most commercial liquid-crystal SLMs is that they are pixelated devices that usually follow the addressing specifications of television or computer displays. According to the VGA format for instance, images of 640 × 480 pixels can be displayed at a 60 Hz frame rate from a computer memory, and the technology is evolving rapidly towards larger pixel counts, say more than 1000 × 1000 pixels. The pixelation has two important consequences. The first is that the

available resolution is ultimately given by the pixel count [3]. The second is that diffraction effects occur because of the physical pixels, i.e. the point spread function depends on the actual size and shape of the pixels.

Fig. 2 shows the basic structure of a pixelated LC-SLM, e.g. an electrically addressed LCTV. Pixels are represented by an aperture function $p(s)$ identical for all pixels but for a translation. For instance the pixels are often rectangular, in which case

$$p(s) = \mathrm{rect}(s/a), \tag{2}$$

where a is the width of the pixel. The pixels are centered at points mb, where b is the pixel pitch, and pixel number m has complex amplitude transmission $t(m)$. If there are N pixels, the width of the SLM is Nb. The SLM pupil function can be written as

$$f(s) = \sum_m t(m)\, p(s - mb), \tag{3}$$

where the summation is over all SLM pixels. In fact in the previous equation only one term of the summation at most is non-null for a given point s of the pupil, i.e. the pixels are non-overlapping. Eq. (3) is fundamental for the problem considered, since it accounts for the transition from the discrete representation $t(m)$ of the SLM image, as stored for instance in a computer memory, to its continuous representation $f(s)$, taking into account explicitly sampling effects.

Upon defining the Fourier transform by

$$\tilde{f}(u) = \int \exp(-2i\pi su)\, f(s)\, \mathrm{d}s, \tag{4}$$

and the inverse Fourier transform by

$$f(s) = \int \exp(2i\pi su)\, \tilde{f}(u)\, \mathrm{d}u, \tag{5}$$

the incoherent PSF in the case of perfect focus can be written as

$$|P(x')|^2 = \left| \tilde{f}\left(\frac{x'}{\lambda z'} \right) \right|^2, \tag{6}$$

where using Eq. (3) and the notation $u = x'/\lambda z'$,

$$\tilde{f}(u) = \left[\sum_m t(m) \exp(-2i\pi mbu) \right] \tilde{p}(u). \tag{7}$$

The latter expression allows to separate the influences of the geometrical shape of the pixels from the SLM transmission

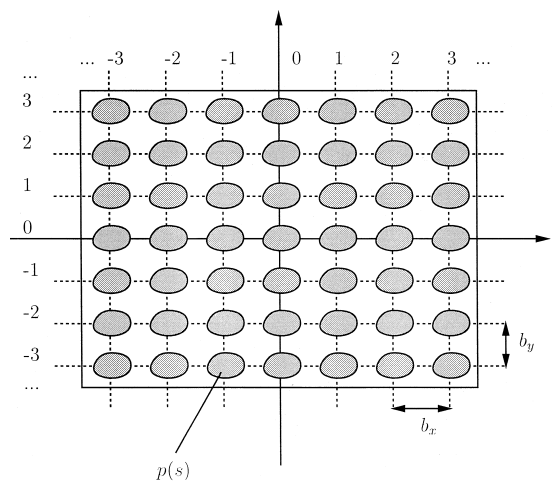

Fig. 2. Notations for the spatial light modulator (SLM).

$t(m)$. Obviously, since the pixels are generally very small, the extension of the function $\tilde{p}(u)$ is very broad. In the particular case of rectangular pixels

$$\tilde{p}(u) = a\,\mathrm{sinc}(au)\,. \tag{8}$$

The first term in Eq. (7) is a continuous version of the discrete Fourier transform of the discrete image $t(m)$

$$\tilde{t}(u) = \sum_m t(m)\exp(-2i\pi mbu)\,. \tag{9}$$

Indeed, for the sampling points n defined by $bu = n/N$ and for these points only, the discrete Fourier transform of $t(m)$ is obtained:

$$\hat{t}(n) = \sum_m t(m)\exp\left(-2i\pi\frac{mn}{N}\right). \tag{10}$$

The function $\tilde{t}(u)$ is periodic, with a period $1/b$. Since only on-axis diffractive control of the PSF is required, this means that energy is lost in higher diffraction orders. The 0 order extends over $-1/2$ to $+1/2$ in the variable bu, and has exactly N resolution cells, i.e. there are as many resolution cells in the PSF as SLM pixels in the pupil plane. The function $\tilde{p}(u)$ merely acts as an envelop limiting the energy lost in higher diffraction orders. In the particular case of a uniform image written onto the SLM ($t(m) = 1$),

$$\tilde{t}(u) = \frac{\sin(\pi Nbu)}{\sin(\pi bu)}\,, \tag{11}$$

The width at half maximum of the function $\tilde{t}(u)$ is then approximately $\Delta u = 1/Nb$, and is consistent with the fact that there are N resolution cells in the PSF.

2.2. Image shifting and focus control

The problem of image shifting, or beam steering, is to shift the point spread function from the optical axis to an arbitrary location x'_0 in the image plane. This can be done without energy loss if the following pure-phase image can be written onto the SLM

$$t(m) = \exp(2i\pi mb\upsilon)\,, \tag{12}$$

where $\upsilon = x'_0/\lambda z'$, for using Eq. (9)

$$\tilde{t}(u) = \frac{\sin(\pi Nb(u-\upsilon))}{\sin(\pi b(u-\upsilon))}\,, \tag{13}$$

i.e. the unperturbed point spread function of Eq. (11) is obtained, but shifted to the desired location x'_0. The maximal resolution available with the SLM, i.e. $\lambda z'/Nb$ is conserved in the shift. The solution of Eq. (12) is the optimal solution for image shifting, before a particular actual SLM coding domain is considered. It is worthwhile noting that the function $\tilde{t}(u)$ is periodic in υ, with a period $1/b$, i.e. the image shifting is identical in every diffraction order and the maximum possible shift is limited by the central diffraction order extension. There is no limitation on the shift υ inside the central diffraction order, and moreover the shift is continuous and not restricted to discrete values, even though the SLM pixel pixel number is finite.

Consider a numerical example with the imaging system parameters given in Table 1. The numerical figures given there are those of the experiments reported below. The distance between adjacent diffraction orders created by the pixelated structure of the SLM is $\lambda z'/b = 4.75$ mm in both X and Y directions. These dimensions define the useful portion of the image formed on a 2D CCD array for instance. The resolution inside the central diffraction order is exactly 640×480 points, or 7.4 μm and 9.9 μm in the X and Y directions respectively. Fig. 3 shows two examples of phase images for shifts

Table 1
Dimensions for the pixelated twisted-nematic liquid-crystal active lens

λ	632.8 nm
z′	300 mm
$N_x \times N_y$	640×480
$b_x = b_y$	40 μm
dimensions	2.56 cm × 1.92 cm

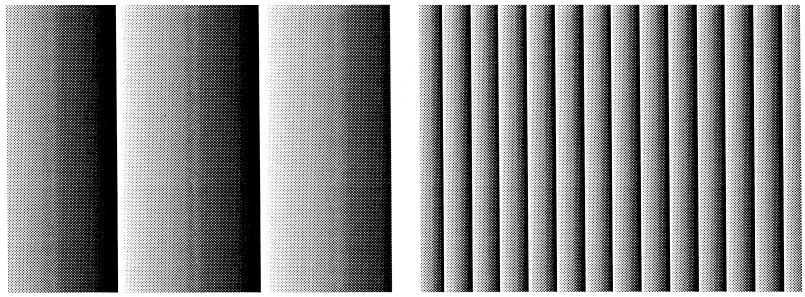

Fig. 3. Examples of simulated 640 × 480 SLM images (continuous pure-phase modulation) for image shifting. Left: 20 μm shift; right: 100 μm shift.

of 20 μm and 100 μm respectively. Fig. 4 shows the numerical simulation of the PSF and of the MTF in the case of 100 μm shift. Note that since the pupil aperture is rectangular, the MTF is trapezoidal. The PSF and MTF were computed using the formulas given in Section 6.

In order to change the longitudinal position of the image plane by a given amount, it is practical to start from Eq. (1) giving the point spread function for a defocus in the Fresnel-Kirchoff approximation of diffraction. If $f(s) = 1$, this expression is that of the amplitude observed at distance $(1 - \epsilon)z'$ instead of z'. Of course if the object is still at distance z, a blurred image will be observed. To put the image back into focus at the distance $(1 - \epsilon)z'$, the SLM image should be

$$f(s) = \exp\left(- \frac{i\pi\epsilon}{(1-\epsilon)\lambda z'} s^2 \right). \tag{14}$$

This is the optimal solution for focus control, but it requires a continuous control of the phase in the pupil plane, i.e. a continuous Fresnel lens. The next classical step is to sample the Fresnel lens at the SLM pixel rate to obtain [16]

$$t(m) = \exp\left(- \frac{i\pi\epsilon}{(1-\epsilon)\lambda z'} (mb)^2 \right). \tag{15}$$

It should be noted however that the function $f(s)$ given by Eq. (14) never complies with the Nyquist criterion for any sampling rate, so that the rough sampling of Eq. (15) always introduces aliasing. Figs. 5 and 6 show numerical simulations of PSFs and MTFs for the parameters of the optical system given in Table 1, together with the corresponding SLM images. If $|\epsilon|$ becomes very large, then instead of the desired central lens many ''secondary lenses'' appear at predictable locations and with predictable focal lengths and energies [15]. A rough estimation of the range of defocus that is achievable with limited aliasing can be obtained simply [3]. Combining image transverse and longitudinal shift can be achieved easily using the following SLM image:

$$t(m) = \exp\left(\frac{2i\pi}{(1-\epsilon)\lambda z'} mbx'_0 \right) \exp\left(- \frac{i\pi\epsilon}{(1-\epsilon)\lambda z'} (mb)^2 \right) \tag{16}$$

2.3. Quantization ghosts

As presented in Section 2.2, continuous pure-phase images are necessary in order to implement exactly the image shifting and focus control functions. However, only a discrete number of grey levels are usually available with a given display

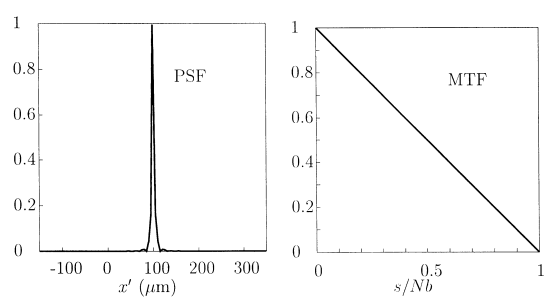

Fig. 4. Numerical simulation of the point spread function (PSF) and modulation transfer function (MTF) for a 100 μm shift.

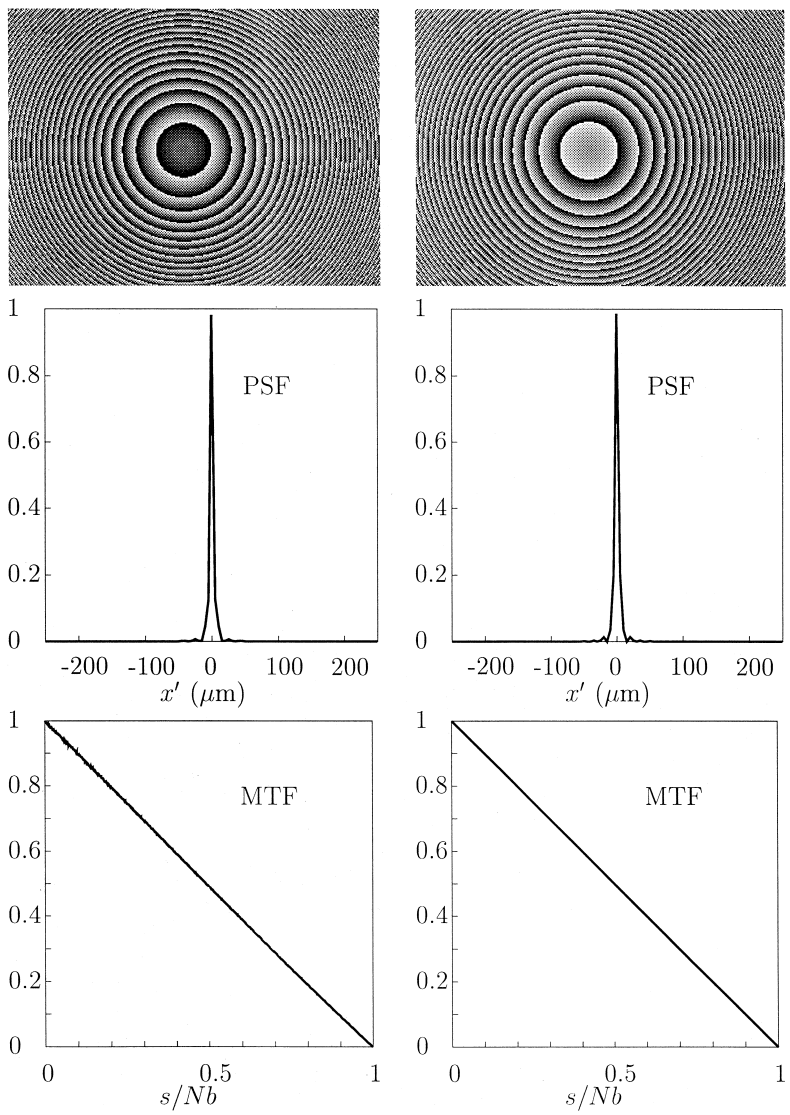

Fig. 5. Examples of simulated 640×480 SLM images (continuous pure-phase modulation) for focus control, and corresponding PSFs. First column: 5% defocus; second column: -5% defocus.

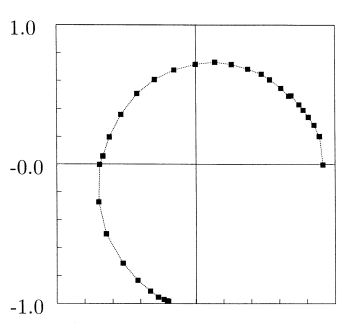

Fig. 6. Measured amplitude and phase modulation for the twisted-nematic LC-SLM used in the experiments for a 632.8 nm wavelength.

device. These grey levels yield discrete phase and amplitude points in the modulation characteristics of the device, and these points have to be used to encode the desired continuous phase image. For instance, these modulation points are shown in Fig. 6 for the particular LC-SLM used in this work, and their experimental determination is reported in Section 3. Dallas [24] has given an elegant answer to the quantization problem, and this section summarizes his results in the active lens context. Closely related works have reported on the effects of phase quantization of Fresnel lenses encoded in pixelated SLMs [25] and on the effects of non-linearities in the SLM characteristics on the performance of kinoforms [26].

Let $\varphi(m)$ be the sampled phase image that has to be written onto the SLM for every pixel m. The ideal transmission of the device or pupil function should then be

$$t(m) = \exp(i\varphi(m)). \tag{17}$$

Only p quantization levels are available. Now every phase value has to be replaced by one of these p quantized complex values. The usual way to do this is to use Euclidean projection $P[\varphi]$, i.e. choose the quantization point that is closest in distance. This Euclidean projection operator is a 2π periodic function of φ, for which a Fourier series expansion can be considered

$$P[\exp(i\varphi)] = \sum_{k=-\infty}^{\infty} G_k \exp(ik\varphi), \tag{18}$$

where the coefficients G_k are defined as

$$G_k = \frac{1}{2\pi}\int_0^{2\pi} \mathrm{d}\varphi\, P[\exp(i\varphi)] \exp(-ik\varphi). \tag{19}$$

The coefficients G_k once they have been computed allow for the quantization effects onto the PSF to be evaluated. Indeed

$$P[t(m)] = \sum_{k=-\infty}^{\infty} G_k \exp(ik\varphi(m)) = \sum_{k=-\infty}^{\infty} G_k\, t^k(m). \tag{20}$$

In case of perfect focus the PSF is proportional to the squared modulus of the Fourier transform (FT) of the pupil function. From the linearity of the FT and of Eq. (18) it comes

$$\mathrm{FT}(P[t]) = \sum_{k=-\infty}^{\infty} G_k\, \mathrm{FT}(t^k). \tag{21}$$

Making use of the convolution theorem, it holds moreover that

$$\mathrm{FT}(t^k)(u) = \begin{cases} \mathrm{FT}(t)(u) \underset{k \text{ times}}{*\cdots*} \mathrm{FT}(t)(u) & \text{if } k>0, \\ \mathrm{FT}(t)(-u) \underset{k \text{ times}}{*\ldots*} \mathrm{FT}(t)(-u) & \text{if } k<0, \end{cases} \tag{22}$$

where $*$ denotes the convolution of two functions. The final result for the effect of quantization is that the coherent PSF expresses as a weighted combination of order k auto-convolutions of the coherent PSF in the unquantized case. The physical meaning of order k auto-convolutions of the coherent PSF is the following. Order 1 (with weight G_1) represents the desired PSF. Indeed, in the case of pure-phase coding (no quantization), $P[\exp(i\varphi)] = \exp(i\varphi)$ and from Eq. (19) it is seen that $G_1 = 1$ and $G_k = 0$ for all $k \neq 1$. Order 0 (with weight G_0) represents the undiffracted light, and the associated coherent PSF $\mathrm{FT}(t^0)$ is the one that would be obtained if the SLM were not present. Orders larger than 2 and smaller than -1 represent ghosts similar to the ghosts that arise classically in ruled gratings when periodic errors occur.

In order to be more specific, the ghosts that appear with image shifting and focus control are considered now. The sampled phase function that is necessary to shift the PSF by a given amount is given by Eq. (12), where v is the spatial frequency yielding the shift $\lambda z' v$ in the detection plane. The kth power of this phase image is

$$t^k(m) = \exp(2i\pi mbkv), \tag{23}$$

and is obviously the phase image yielding a shift of kv. Thus, the quantization of a ''prism image'' creates an infinite number of ghosts, each with intensity $|G_k|^2$, repeating the PSF along the line defined by the desired shift v. The effect on the observed image will that of a replication of the original image (see Sections 4 and 5 for experimental examples of this effect). Of course, these ghosts will be appreciable and disturbing only if their intensities $|G_k|^2$ cannot be neglected. In any case, it is preferable to have $|G_1|^2$ as close to unity as possible.

Table 2
$|G_k|^2$ coefficients for the twisted-nematic LC-SLM used

	k							
	−3	−2	−1	0	1	2	3	4
$\|G_k\|^2$	0.0085	0.0105	0.0091	0.0004	0.6228	0.0067	0.0007	0.0015

In a similar way, the sampled phase image that is necessary to change the plane of focus from the distance z' to the distance $(1-\epsilon)z'$ is given by Eq. (15). The kth power of this phase image is

$$t^k(m) = \exp\left(-\frac{i\pi k\epsilon m^2 b^2}{(1-\epsilon)\lambda z'}\right), \tag{24}$$

and is the sampled phase image yielding focus change to the distance

$$z'\left(1+\frac{k\epsilon}{1-\epsilon}\right)^{-1}. \tag{25}$$

Unlike the image shift case, ghosts appear at different focus planes and are consequently less disturbing since they are non-overlapping. Furthermore the ghost focus planes are not equidistant.

Table 2 gives the intensities of the ghosts for the particular twisted-nematic LC-SLM we used. It should be noted that the $|G_1|^2$ value determines the maximum diffraction efficiency available with a given set of quantization points for implementing a pure-phase SLM image that originally had 100% diffraction efficiency, as is the case for instance for image shifting and focus control. In the case of the twisted-nematic LC-SLM used, the diffraction efficiency is limited to 62%, but there is almost no energy lost in the undesired ghosts, i.e. the residual amplitude modulation is mostly responsible for the decrease in diffraction efficiency.

3. Twisted-nematic LC-SLM modulation measurement

The principle of amplitude and phase modulation with a twisted-nematic LC-SLM has been discussed in many papers recently [8,9,22,27–30] and will not be repeated here. This section rather reports on the measurement method used with the LC-SLM used. The amplitude and phase modulation with nematic LC-SLMs depends mostly on the voltages applied to the pixels, or equivalently on the grey level of the image written onto the SLM. Additional parameters are the angular positions of the two polarizers in the case of twisted-nematic LC-SLMs. Practically, these angular positions can be set either ad hoc in order to obtain the desired amplitude and/or phase modulation, although this is arbitrary and cumbersome, or they can be determined from the Jones matrix of the SLM. The latter solution ensures that the best possible configuration can be found, and this is the one that was chosen for the particular commercial twisted-nematic LC-SLM used. Note that the configuration with the least remaining amplitude modulation, or phase-mostly modulation was looked for.

Even though the Jones matrix for a twisted-nematic LC cell cannot be obtained analytically in general, it can be rather easily obtained experimentally, as was shown by Yamauchi et al. [31], using combinations of amplitude and phase modulation measurements for several angular configurations of the polarizers. The Jones matrix assumes the following form,

$$J = A\exp(-i\beta)\begin{pmatrix} f-ig & -h-ij \\ h-ij & f+ig \end{pmatrix}, \tag{26}$$

where A is the amplitude attenuation of the cell, β is a phase retardation, and the real parameters f,g,h and j are related by the normalization relation

$$f^2+g^2+h^2+j^2 = 1. \tag{27}$$

The expressions for the different parameters are given in Ref. [31] when no voltage is applied to the cell. When a voltage is applied, the expression of the Jones matrix is deeply modified, but as is shown in Appendix A based only on geometrical arguments, the Jones matrix retains the form of Eq. (26) where the real coefficients f,g,h and j are arbitrary but for the normalization relation of Eq. (27). Note that the Jones matrix depends on the grey level.

The measurement of the amplitude modulation is rather easy and precise, and can be obtained for instance by writing a uniform grey level image onto the SLM and measuring the transmitted intensity [28,29]. The phase determination is in

essence interferometric, and many different methods have been proposed in the literature. One simple and reliable but very slow method involves a Mach-Zehnder interferometer [27], used to record the displacement of equal inclination fringes between two grey levels. More recent methods employ a Ronchi grating [30], a wedge shear plate [8] or Young pinholes [9]. In one variant [32], a Ronchi grating is directly written onto the SLM which allows for a very simple and fast implementation. This is the solution that was chosen and that is described in the following.

The method proposed by Zhang et al. [32] in order to estimate the phase associated to each grey level is to write a ''Ronchi grating'' image onto the SLM. This image is made of two alternating lines (or columns) with different grey levels. As the spatial frequency of such a grating is exactly $1/2$ with respect to the pixel pitch, or equivalently the periodicity is two pixels, an incident plane wave is diffracted only in integer diffraction orders and half-integer diffraction orders. A combination of the intensities in the 0 and $1/2$ diffraction orders yields the phase difference between the two grey levels. When compared to the classical interference fringe analysis method, the Zhang method is much faster, since the treatment of a complete interferogram for a single phase measurement is avoided. However, two major concerns have to be taken into account. First the phase estimation precision depends directly on the energy balance between the $1/2$ and 0 diffraction orders; if one of these is too small compared to the other the phase can be indeterminate depending on the noise level. To overcome this problem, a χ^2 (Chi square) estimation method was used as described in the following. Second, the LC-SLM must be able to display exactly a high spatial frequency image. With the VGA type LC-SLM used, it was found that the phase measurement was only valid when the grating lines were along the scan lines of the device.

Using the amplitude and phase measurement principles just described, the Jones matrix of the LC-SLM, as given by the six real parameters A, β, f, g, h and j of Eq. (26), was determined along the following lines. Amplitude and phase measurements were performed for several polarizer angular configurations. To correct for the relative spread of the measurements and obtain a robust estimation scheme, a Chi-square type estimation algorithm was chosen. Specifically the following criterion was minimized over the parameters for each grey level using a gradient algorithm:

$$\chi^2(A,\beta,f,g,h,j) = \sum_i \frac{(v_i - m_i)^2}{v_i}, \tag{28}$$

where v_i and m_i denote respectively the ith measurement and the theoretical value for this ith measurement given the parameters. The output of such an optimization algorithm is an estimate for the Jones matrix that is accepted only if the final value of the Chi-square criterion is sufficiently low. The same approach but with a least-squares criterion led to unstable results.

From the result of the estimation of the Jones matrix, the best polarizer combination was selected, and the amplitude and phase measurements were conducted again for this particular configuration. The results are shown in Fig. 6. As can be seen, the phase modulation depth does not reach 2π, and spurious amplitude variations are still observable. It will be seen however in Sections 4 and 5 that this imperfect phase-mostly modulation allows for good performance of an active lens system.

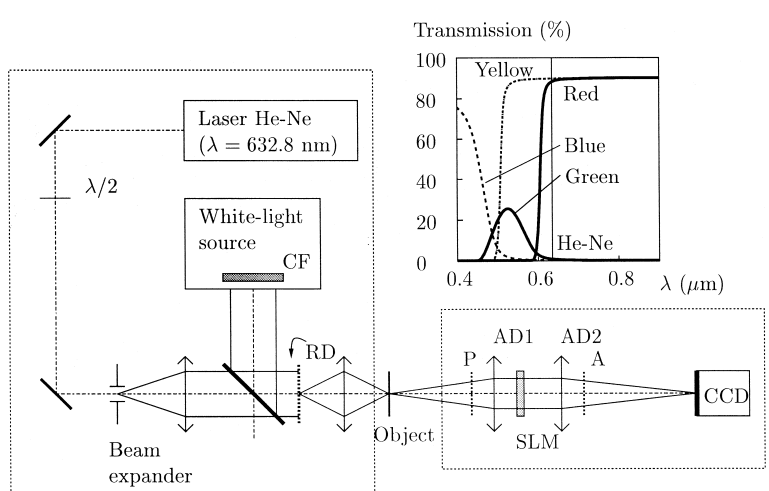

Fig. 7. Schematic of the experimental set-up of the active lens. The curves are for the spectral transmission of the color filters used with the white-light source. CF: color filters; RD: rotating diffuser; P: polarizer; A: analyzer; AD1, AD2: achromatic doublets.

4. Experiments in monochromatic light

The experimental set-up used is depicted in Fig. 7. The schematic is divided into two blocks, one for the illumination of the object and the other for the active lens itself. The illumination can be either a He-Ne laser ($\lambda = 632.8$ nm) or a halogen white-light source. The white-light source can be spectrally filtered with color filters to study chromatism as described in the next section. The transmission spectra of the color filters are shown in Fig. 7. The object in the experiments reported is a resolution target. It is illuminated indirectly by a rotating diffuser which is a circular piece of ground glass driven by a rotating engine. The rotating diffuser is used to wash out the speckle when laser illumination is used. The imaging system is made of two achromatic doublets corrected for spherical aberration with respectively focal lengths of 200 mm and 300 mm. The object is in the object focal plane of the first doublet and the CCD camera is in the image focal plane of the second doublet. The pixel pitch of the CCD sensor is 14×14 μm^2. The SLM is placed somewhere in between the two doublets and defines the pupil plane of the imaging system. The exact position of the SLM is irrelevant in first approximation. The images

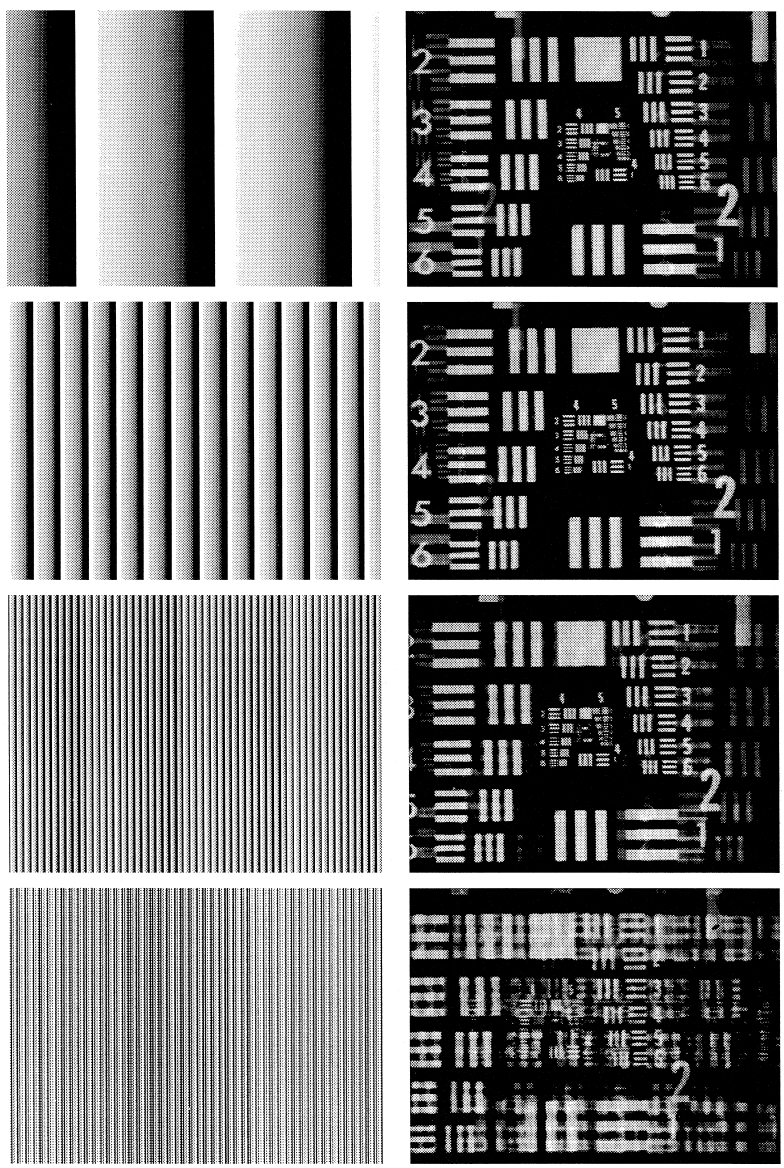

Fig. 8. Horizontal image shifting. The left column shows the phase images written onto the SLM, and the right column shows the experimental images obtained. From top to bottom, 20 μm shift, 100 μm shift, 400 μm shift and 1000 μm shift.

shown in Figs. 8–11 and 13 were acquired using a frame grabber with 640×480 pixels and 8 bits of resolution (VGA format).

Figs. 8 and 9 show examples of horizontal and vertical image shifting respectively. The phase images written onto the SLM are shown in the left column and the shifted images obtained experimentally are shown in the right column. The higher order diffraction orders that are due to the pixelated nature of the SLM are clearly visible and appear with an energy less than the useful central diffraction order, as expected. In addition to the higher order diffraction orders, there appear ghosts arising from a complicated combination of aliasing and quantization. Such a ghost can be clearly seen in Fig. 9, last line, with the resolution target replicated just above its shifted image. Furthermore, it is seen that the quality of the shifted images degrades as the amount of shift requested increases, or equivalently as the spatial frequency of the ''prisms'' written onto the SLM increases. Significantly, the quality of image shifting is much higher vertically than horizontally, even though the number of pixels is higher in the horizontal direction (680 pixels) than in the vertical direction (480 pixels). This is a direct consequence of the addressing scheme, i.e. VGA signals, used for displaying the phase image onto the SLM. Similar

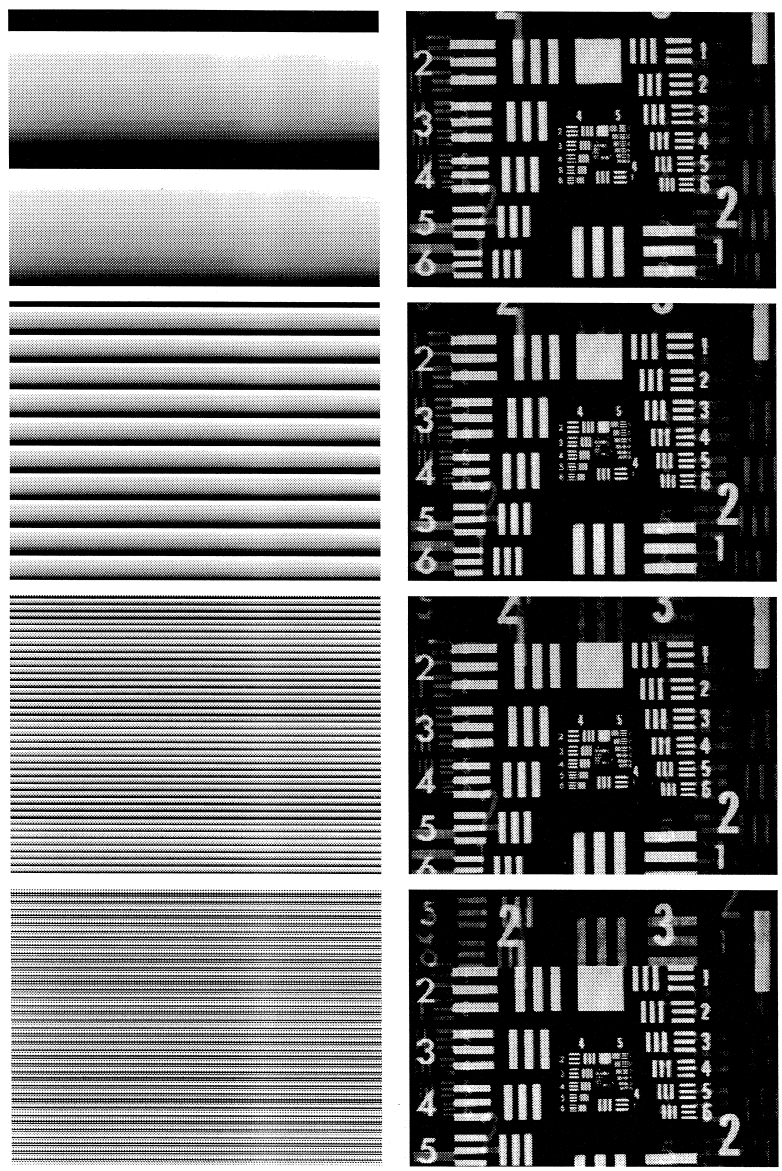

Fig. 9. Vertical image shifting. The left column shows the phase images written onto the SLM, and the right column shows the experimental images obtained. From top to bottom, 20 μm shift, 100 μm shift, 400 μm shift and 1000 μm shift.

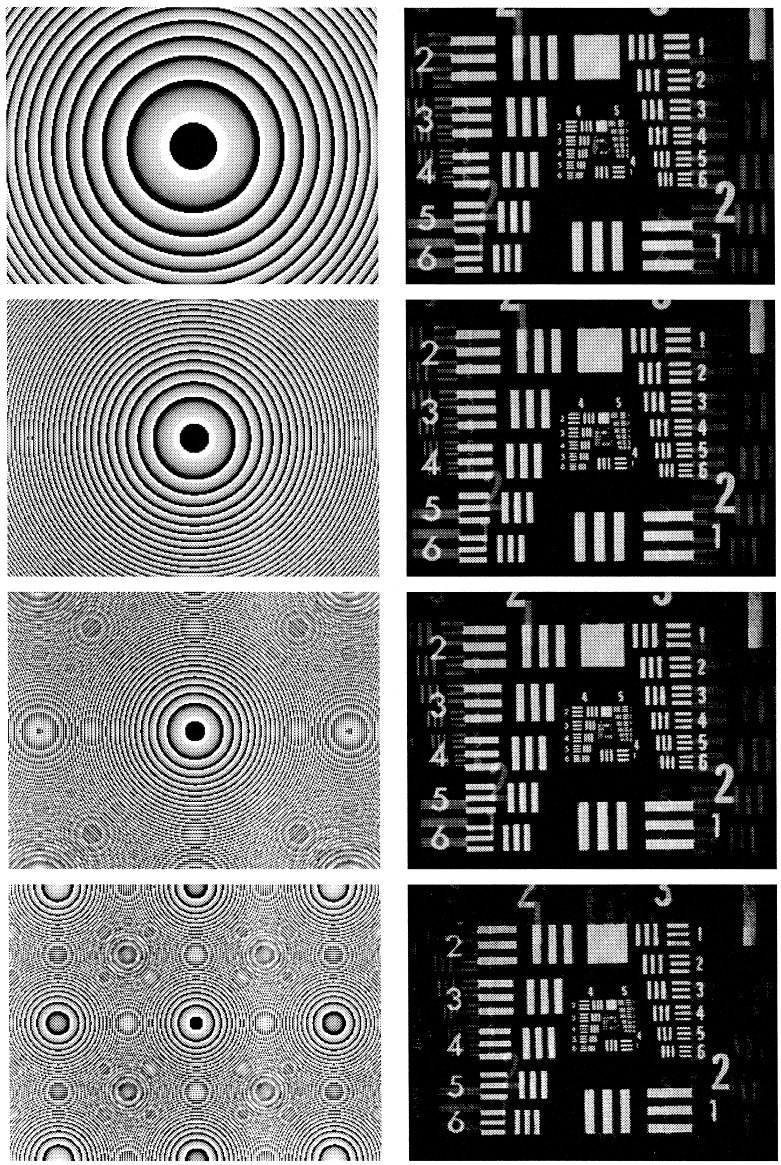

Fig. 10. Positive focus control. The left column shows the phase images written onto the SLM, and the right column shows the experimental images obtained. From top to bottom, 2%, 5%, 10% and 20% defocus.

experiments with a SLM controlled by video CCIR signals showed even worse results. This limitation is purely technological, and would be relieved if a real pixel by pixel addressing scheme were used. Anyway, it is encouraging to see that a phase-mostly modulation limited to $3\pi/2$ approximately is enough to obtain good quality results. With a pure-phase SLM, e.g. using parallel aligned nematic liquid-crystals and the same number of pixels, the results would probably be even better. Interestingly, it can be seen that small shifts can be achieved with very few resolution losses and with almost all the energy diffracted correctly at the shifted location, i.e. the energy of the ghosts is small as predicted.

Similar experiments on image shifting were reported by Takaki et al. (Fig. 11 of Ref. [3]) using a pure-phase SLM with 236×105 pixels and white-light illumination. Their results show a more rapid degradation of the image resolution with the requested image shift. This can be attributed to the wide wavelength range of their illumination, although the chromatism results of next section demonstrate that this effect is not so important, but more significantly this indicates that the number of pixels in the SLM is the most important factor determining the quality of the final result, as expected from a theoretical analysis of sampling effects.

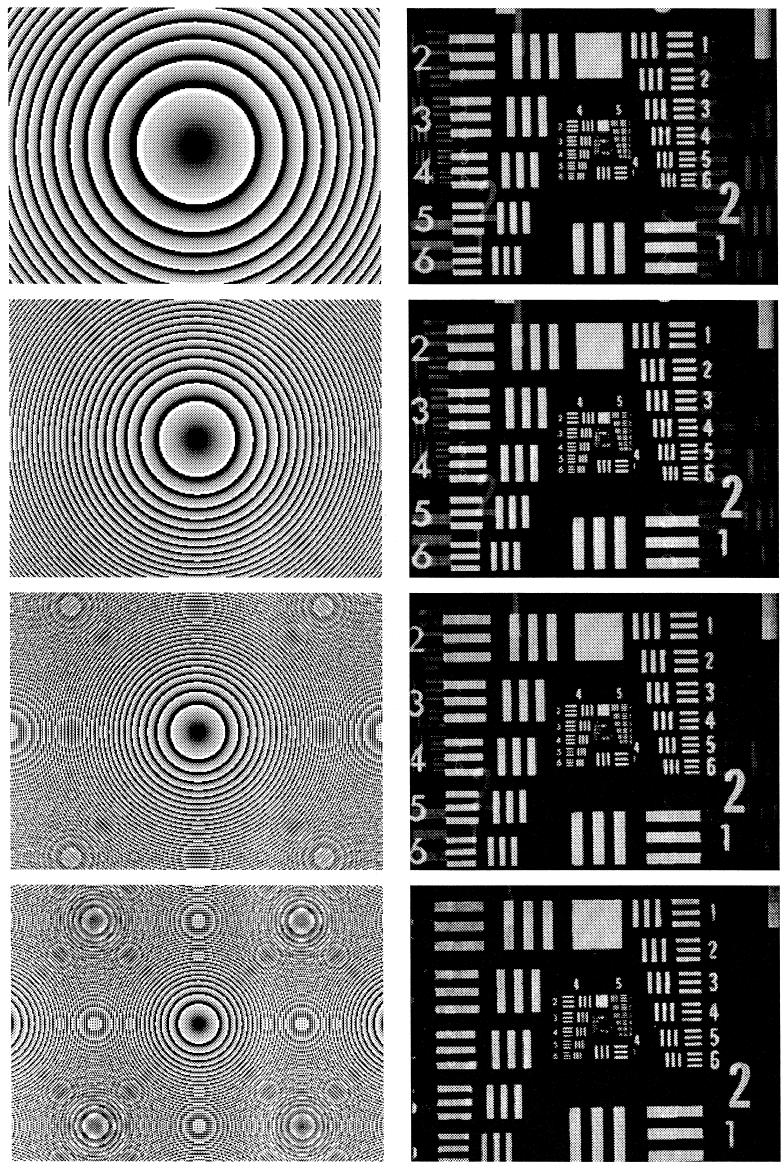

Fig. 11. Negative focus control. The left column shows the phase images written onto the SLM, and the right column shows the experimental images obtained. From top to bottom, −2%, −5%, −10% and −20% defocus.

Figs. 10 and 11 show examples of positive and negative focus control respectively. The experimental images were acquired after translation of the CCD camera to obtain the best focus plane. As in the case of image shifting, higher diffraction orders are clearly visible, but the effect of increasing spatial frequencies of the ''lenses'' written onto the SLM or equivalently increasing defocus is quite different. The resolution of the defocused image seems almost unaltered for large defocus, but its energy decreases. This can be understood by an energy spreading due to the multiple lenses that appear in a sampled Fresnel lens when a small focal length is requested [15], as can be seen in Figs. 8 and 9. It can also be seen that the image size increases with negative defocus and decreases with positive defocus, as it should from geometrical optics. The amount of defocus that it is possible to generate with negligible aliasing is limited to the −10% to 8% range with the set-up used. As in the case of image shifting, though they are less visible, there appear additional ghosts arising from a complicated combination of aliasing and quantization. Such a ghost can be clearly seen in Fig. 10, last line, with the resolution target replicated just above its shifted image.

5. Chromatism

Up to now, only monochromatic illumination has been considered. In this section, the practically interesting case of temporally incoherent illumination, e.g. as obtained from a white-light source, is considered. This situation can be described mathematically as a continuous wavelength spectrum centered around λ_0, such that all the PSFs created by individual wavelengths add incoherently, i.e. in intensity. Three different chromatism effects can be identified, refractive index chromatism, diffraction chromatism and quantization chromatism. The first is characterized by the wavelength dependence of the refractive index of the liquid-crystal, and is the usual dispersion. The second is associated to diffraction, namely because the PSF depends explicitly on the wavelength. The third is created by quantization effects, and more specifically results from the definition modulo-2π of the phase image written onto the SLM.

The first kind of chromatism, refractive index chromatism, is a very classical subject in optical system design, and will not be discussed in this paper, so that the ordinary and extraordinary refractive indices n_o and n_e are considered at least approximately constant in the following. The second kind of chromatism, diffraction chromatism, has indeed no effect on the function achieved by an active lens, since the physical effect used is mostly a modulation of the index of refraction in the depth of the liquid crystal. This results from the fact that the relevant quantity is the variation of optical path, and not the phase modulation, which is the previous quantity multiplied by $2\pi/\lambda$, although this distinction was not necessary in the monochromatic case. This is exactly the situation with usual bulk glass prisms or lenses.

Fig. 12a illustrates the problem arising in polychromatic light from the quantization modulo-2π of a pure-phase image. Indeed, if the image is reset to 0 when 2π is reached for wavelength λ_0, the phase reached before reset will be higher

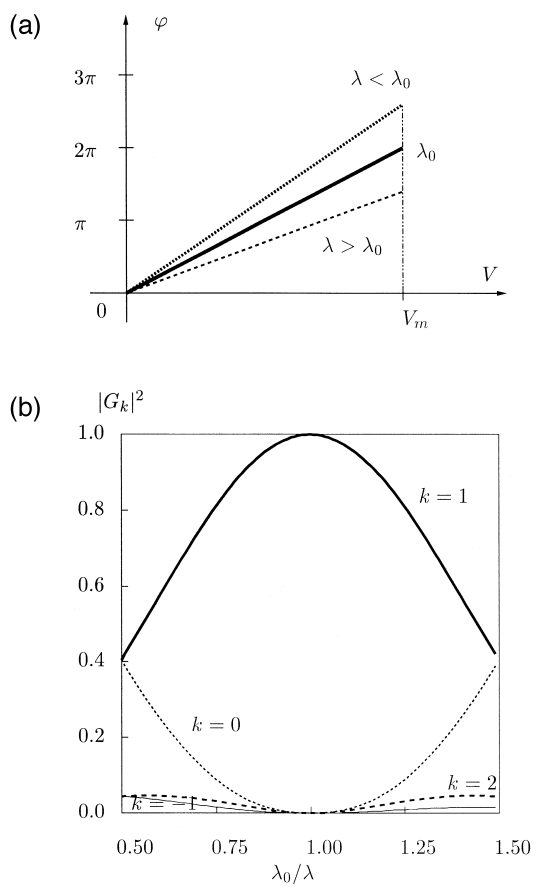

Fig. 12. Quantization chromatism, that is due to the modulo-2π definition of phase: (a) deformation of the phase encoded as a function of the voltage applied to the LC cell; (b) intensity $|G_k|^2$ of the kth ghost as a function of wavelength.

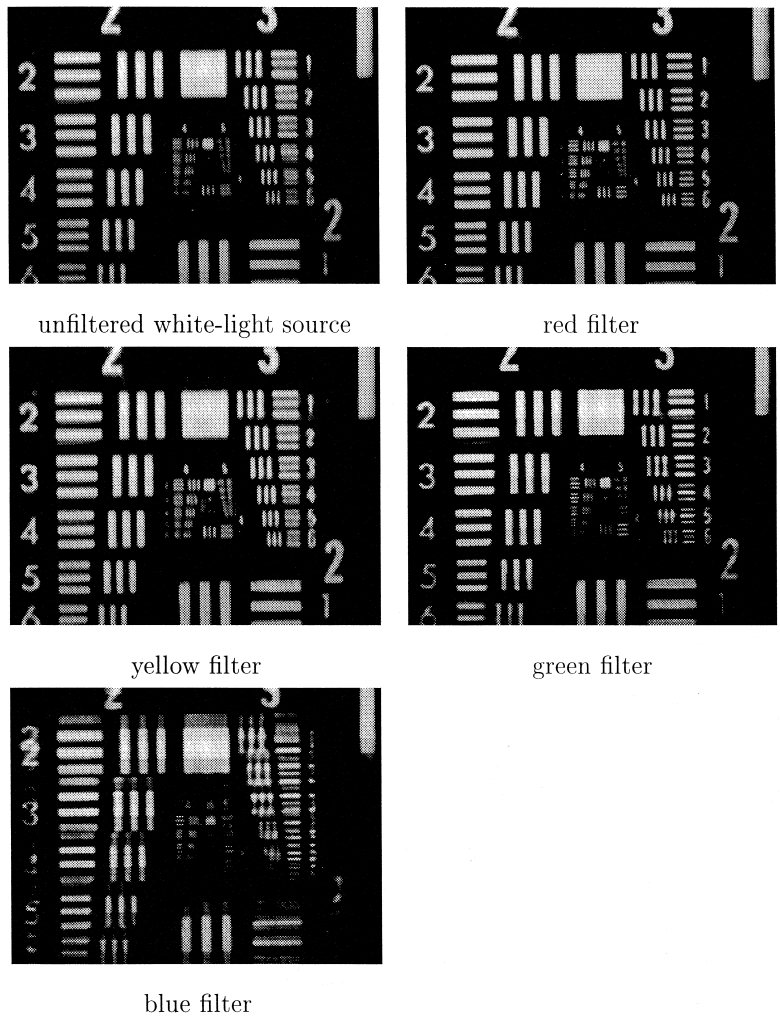

Fig. 13. Examples of images obtained using white-light illumination showing the effect of chromatism. The white-light source is a halogen lamp spectrally filtered by color filters whose spectra are shown in Fig. 7. The SLM phase image used is shown in Fig. 9, third row, and produces a 400 μm vertical shift.

(lower) for a wavelength smaller than (larger than) λ_0. If $V_{\max}$ denotes the voltage applied to reach 2π phase modulation at λ_0 and assuming the modulation is mostly that of the index of refraction,

$$\Delta\varphi(V_{\max}) = 2\pi = 2\pi\frac{\Delta n(V_{\max})e}{\lambda_0}, \tag{29}$$

and then for any other wavelength λ

$$\Delta\varphi(V_{\max}) = 2\pi\frac{\Delta n(V_{\max})e}{\lambda} = 2\pi\frac{\lambda_0}{\lambda}. \tag{30}$$

Now the description of quantization effects of Section 2.3 can be applied with the Euclidean projection given by

$$P[\exp(i\varphi)] = \exp\left(i\frac{\lambda_0}{\lambda}\varphi\right). \tag{31}$$

From this expression, the G_k coefficients are easily calculated to be

$$G_k = \exp\left(i\pi\frac{\lambda_0}{\lambda}\right)\frac{\sin(\pi\lambda_0/\lambda)}{\pi(\lambda_0/\lambda - k)}. \tag{32}$$

Fig. 12b shows how the intensity $|G_k|^2$ of the kth ghost evolves as a function of wavelength. When $\lambda = \lambda_0$ only the first ghost is present, i.e. the desired phase function is perfectly encoded. In the vicinity of λ_0, the intensities of the other ghosts increase gradually, and imply a corresponding decrease in the first ghost intensity, but only the $k = 0$ ghost is truly significant if the relative bandwidth does not exceed a reasonable value, say 20%.

Fig. 13 shows experimental examples of a 400 μm vertical image shifting for the unfiltered spectrum (extending roughly from 350 nm to 1 μm, with more energy in the red than in the blue), and the spectrally filtered spectra. It can be observed that the ghosts appear very faintly, if they can only be detected, except for the blue light illumination where the $k = 0$ ghost is clearly visible. It should be stressed that the blue filtered spectrum centered somewhere around 400 nm is very far from the optimization $\lambda_0 = 632.8$ nm wavelength, and this observation confirms that quantization chromatism is not too much disturbing over quite extended spectra. With unfiltered white light source, the $k = 0$ ghost is not visible whereas it is using the blue filter. Indeed it is present with unfiltered white light source, but relatively less important since the lamp spectrum is mainly red. It can be observed also that the resolution of the image seems quite diminished compared to that of the corresponding monochromatic image of Fig. 9, third row. This can be explained from the residual chromatism of the doublets used, the refractive index chromatism of the liquid-crystal that was not taken into account, and the fact that the Jones matrix for a twisted-nematic LC cell depends in a complicated way on the wavelength, so that diffraction chromatism may still be present. Specifically, the image obtained with the yellow filter seems more blurred than that obtained with the red or green filters. This is due to the spectral bandpass of the yellow filter which is wider than that of the other filters. One additional and interesting effect is that the higher diffraction orders that were present in the experimental examples of Figs. 8 to 11 vanish in the polychromatic case. This occurs because these diffraction orders are created by diffraction by the pixel matrix of the SLM so that their angular positions are highly chromatic, whereas the position of the central diffraction order is not. These higher diffraction orders are consequently still present but highly spread spatially so that they are not detected.

6. Numerical evaluation of the PSF and the MTF

6.1. Point spread function

The numerical evaluation of the PSF in the perfect focus case (Eq. (7)) has the following characteristics. The envelop term $\tilde{p}(u)$ is generally easily computed, and has an especially simple form in the case of rectangular pixels. The discrete Fourier transform $\hat{t}(n)$ of the SLM image is best computed using a FFT algorithm, that requires approximately $2N\log(N)$ operations for obtaining simultaneously the N equidistant sampling points in the central order of diffraction. If the PSF is needed in between the previous sampling points, no fast exact algorithm exists, and the summation of Eq. (7) requires N operations per desired point. This computation is necessary to reveal details of the PSF that are finer than the sampling grid.

In the case of defocus, there is no fast algorithm like the FFT for computing the PSF. An approximate method is sometimes found in the literature that replaces the continuous Gaussian term in Eq. (11) by its sampled expression. Then the PSF is simply given by the discrete Fourier transform of the product of the SLM pupil function with the sampled Gaussian term. This method cannot be recommended since a imaginary Gaussian does not fulfill Shannon's condition for any sampling rate, and it gives correct results only for very small defocuses. However the computation time of the Fresnel integral in Eq. (11) can be shortened without need for an approximation [33]. Using Eqs. (15) and (16) we obtain

$$P(x') = B\sum_m t(m)\int \mathrm{d}s\, p(s-mb)\exp\left(\frac{i\pi(\epsilon s^2 - 2sx')}{\lambda z'(1-\epsilon)}\right), \tag{33}$$

where B is a normalization constant. By convention, the PSF is normalized on the axis ($x' = 0$), for a uniform SLM image ($t(m) = 1$), and for perfect focus ($\epsilon = 0$). Then $B^{-1} = N|\tilde{p}(0)| = Na$, i.e. the inverse of the useful surface of the SLM. Useful formulas are indicated now in the case of rectangular pixels for practical convenience. Calculations are cumbersome, but merely consist in variable exchanges. In the case of perfect focus ($\epsilon = 0$)

$$P(x') = \frac{1}{N}\,\mathrm{sinc}(au)\sum_m t(m)\exp(-2i\pi mbu), \tag{34}$$

with $u = x'/\lambda z'$. In the case of over-focus ($\epsilon > 0$)

$$P(x') = \frac{1}{N}\sum_m t(m)\Psi(\alpha,\beta), \tag{35}$$

and in the case of under-focus ($\epsilon < 0$)

$$P(x') = \frac{1}{N}\sum_m t(m)\Psi^*(\alpha,\beta), \tag{36}$$

with

$$\alpha = \frac{a^2}{\lambda z'}\frac{\epsilon}{1-\epsilon}, \tag{37}$$

$$\beta = mb/a - x'/(\epsilon a), \tag{38}$$

$$\Psi(\alpha,\beta) = \frac{1}{\alpha}(\psi(\alpha(\beta+1/2) - \psi(\alpha(\beta-1/2)))), \tag{39}$$

$$\psi(\gamma) = \int_0^\gamma \exp(i\pi t^2)\,\mathrm{d}t. \tag{40}$$

$\psi(\gamma)$ is the Fresnel integral, a special function for which series and asymptotic expansion are known [34]. It is then convenient to tabulate the function $\Psi(\alpha,\beta)$ or alternatively the Fresnel integral to compute the PSF in the defocus case. The computation complexity is then N operations per desired point. For other pixel shapes, it is possible to obtain similar expressions involving the Fresnel transform of the pixel function appearing in Eq. (33). Approximation methods for the fast evaluation of Fresnel type diffraction integrals can be found in Ref. [35].

6.2. Modulation transfer function

The modulation transfer function (MTF) is given in the cases of in-focus and out-of-focus by [1]

$$\mathrm{MTF}(s) = \frac{\left|\int \mathrm{d}s'\, f^*(s')f(s+s')\exp(2i\pi\epsilon s\cdot s'/\lambda z'(1-\epsilon))\right|}{|[f\otimes f](0)|}, \tag{41}$$

where the autocorrelation of the pupil function is defined by $[f\otimes f](s) = \int f^*(s')f(s+s')\mathrm{d}s'$. Eq. (41) simplifies to the well-known form $\mathrm{MTF}(s) = |[f\otimes f](s)|/|[f\otimes f](0)|$ if $\epsilon = 0$. In this case

$$[f\otimes f](s) = \sum_k\sum_m t^*(k)t(m)[p\otimes p](s+(k-m)b). \tag{42}$$

The support of $[p\otimes p]$ is contained in $[-a,a]$, itself included in $[-b,b]$. Then

$$-a \le s + (k-m)b \le a. \tag{43}$$

These conditions imply that at most 2 points k exist for a given point m (and 4 points in the 2D case). Then there are at most $2N$ terms in the summation, but Eq. (42) does not simplify further in the general case. In the case of rectangular pixels, the autocorrelation $[p\otimes p]$ is a trapezoidal function with unit height and with $[-a,a]$ as basis. A simpler formula can be found if the MTF is evaluated only at the SLM pixels centers. After some algebra it can be shown that

$$\mathrm{MTF}(kb) = \frac{1}{N|\tilde{p}(0)|}\left|\tilde{p}\left(\frac{\epsilon kb}{\lambda z'(1-\epsilon)}\right)\sum_m t^*(m)t(m+k)\exp\left(\frac{2i\pi\epsilon b^2 mk}{\lambda z'(1-\epsilon)}\right)\right|, \tag{44}$$

where the summation must be understood for pixels m such that $|m+k| \le N$. Furthermore, in the case of rectangular pixels

$$\mathrm{MTF}(kb) = \frac{1}{N}\,\mathrm{sinc}(\alpha bk/a)\left|\sum_m t^*(m)t(m+k)\exp\left(2i\pi\alpha\frac{b^2}{a^2}mk\right)\right|. \tag{45}$$

Whatever the pixel shape, expression (44) reduces in the case of perfect focus ($\epsilon = 0$) to

$$\mathrm{MTF}(kb) = \frac{1}{N}\left|\sum_m t^*(m)t(m+k)\right|. \tag{46}$$

Eq. (44) can only be evaluated by direct summation over the SLM image for every desired sampling point of the MTF. However Eq. (46) is a discrete correlation, and thus can be advantageously evaluated using the Fast Fourier Transform (FFT).

7. Conclusion

Active or reconfigurable lenses may find useful applications in classical imaging systems, where they can be used to control the optical transfer function in a limited range or to compensate for internal and external aberrations. Pixelated pure-phase SLMs, e.g. electrically addressed phase SLMs, are especially interesting in this respect. The purpose of this paper has been to demonstrate the use of a commercial twisted-nematic liquid-crystal SLM as a phase-mostly modulator in an active lens system. The analysis was applied to the practical cases of image shifting (or beam steering) and of focus control. Provided a perfect pure-phase modulation is available, any shift to within the central diffraction order can be achieved, while the range of defocus that can be achieved is limited by aliasing.

In the context of active lenses, the quantization effects that arise from limited modulation capabilities, i.e. departure from continuous pure-phase modulation, were investigated using a method due to Dallas [24]. This method was also used to describe the action of chromatism, related to the modulo-2π definition of phase. A practical and accurate procedure was described for the experimental estimation of the Jones matrix of a twisted-nematic LC-SLM as a function of grey level. The method basically combines results of Refs. [31] and [32] with a robust parameter estimation algorithm. An experimental set-up of an active lens system was then presented, together with experimental examples in monochromatic light of image shifting and focus control. The experimental images obtained show that the quality and the resolution of the image formed by the active lens system is almost constant over an extended range of shift and/or defocus. For the commercial twisted-nematic LC-SLM used, the ghosts can be neglected in monochromatic light, but the higher diffraction orders are more disturbing. Experimental examples and calculations show that chromatism can be neglected over a relative bandwidth of $\pm 10\%$ approximately. Furthermore, a nice feature of polychromatic illumination is that the higher diffraction orders are washed out, and hence are not as disturbing as with monochromatic illumination. Useful formulas were provided for computing the point spread function and the modulation transfer function for both in-focus and out-of-focus systems.

Acknowledgements

The author acknowledges partial support for this research by the Direction des Recherches et Etudes Techniques, and is grateful to J.-P. Huignard and Ph. Réfrégier for fruitful discussions.

Appendix A. General expression for the Jones matrix of a twisted-nematic LC cell

In order to obtain the general expression of Eq. (26) for the Jones matrix of a twisted-nematic LC cell, an argument given in Ref. [36] can be generalized. When a voltage is applied to the LC cell, the rotation of the liquid crystal molecules is assumed to be homogeneous in each elementary slice parallel to the cell entrance and exit slabs, i.e. each slice is considered a thin plate of a birefringent uniaxial crystal. According to this simplified model, the LC depth can be divided into M slices with associated retardation Γ_k and rotation angle θ_k, k being an index in the range $1,\ldots,M$. The Jones matrix of the LC cell can then be written as [36]

$$J = \prod_{k=1}^{M} R(-\theta_k)\cdot W_k \cdot R(+\theta_k), \tag{A.1}$$

with

$$W_k = \exp(-i\Gamma_k/2)\begin{pmatrix} \exp(-i\Gamma_k/2) & 0 \\ 0 & \exp(i\Gamma_k/2) \end{pmatrix}, \tag{A.2}$$

and where $R(\theta_k)$ is the rotation matrix for rotation angle θ_k defined by

$$R(\theta_k) = \begin{pmatrix} \cos\theta_k & \sin\theta_k \\ -\sin\theta_k & \cos\theta_k \end{pmatrix}. \tag{A.3}$$

It is easily seen that

$$R(-\theta)\cdot W \cdot R(\theta) = \exp(-i\Gamma_k/2)\begin{pmatrix} \cos(\Gamma/2) - i\sin(\Gamma/2)\cos 2\theta & -i\sin(\Gamma/2)\sin 2\theta \\ -i\sin(\Gamma/2)\sin 2\theta & \cos(\Gamma/2) + i\sin(\Gamma/2)\cos 2\theta \end{pmatrix}. \tag{A.4}$$

This unitary matrix assumes the following form

$$\exp(-i\beta)\begin{pmatrix} f-ig & -ij \\ -ij & f+ig \end{pmatrix}. \tag{A.5}$$

It is easy to check that the product of two matrices of the previous form assumes the form of Eq. (26), and hence the product (A.1). Further elementary algebra shows that the matrices assuming this form are stable for matrix multiplication and non-singular since of unitary determinant, so that they have a group structure. The most general form for the Jones matrix of a twisted-nematic LC cell is then given by Eq. (26), irrespectively of the particular retardations Γ_k and rotation angles θ_k involved. This result is not of great help for numerical evaluation of the Jones matrix, but justifies its experimental determination as described in Section 3.

References

[1] J.W. Goodman, Introduction to Fourier Optics, McGraw-Hill, San Francisco, CA, 1968.
[2] Y. Takaki, Proc. Soc. Photo-opt. Instrum. Eng. 2565 (1995) 205.
[3] Y. Takaki, H. Ohzu, Optics Comm. 126 (1996) 123.
[4] Y. Takaki, H. Ohzu, Appl. Optics 35 (1996) 6896.
[5] J. Amako, H. Miura, T. Sonehara, Appl. Optics 32 (1993) 4323.
[6] J. Chen, G. Lai, K. Ishizuka, A. Tonomura, Appl. Optics 33 (1994) 1187.
[7] R. Piestun, J. Shamir, Optics Lett. 19 (1994) 771.
[8] L. Gonçalves Neto, D. Roberge, Y. Sheng, Appl. Optics 34 (1995) 1944.
[9] A. Bergeron, J. Gauvin, F. Gagnon, D. Gingras, H.H. Arsenault, M. Doucet, Appl. Optics 34 (1995) 5133.
[10] P.F. McManamon, E.A. Watson, T.A. Dorschner, L.J. Barnes, Opt. Eng. 32 (1993) 2657.
[11] R.J. Broessel, V. Dominic, R.C. Hardie, Opt. Eng. 34 (1995) 3138.
[12] E.C. Tam, S. Zhou, M.R. Feldman, Appl. Optics 31 (1992) 578.
[13] E.C. Tam, Optics Lett. 17 (1992) 369.
[14] J.A. Davis, H.M. Schley-Seebold, Appl. Optics 31 (1992) 6185.
[15] E. Carcolé, J. Campos, S. Bosch, Appl. Optics 33 (1994) 162.
[16] R. Silvennoinen, J. Uozumi, T. Asakura, J. Optics (Paris) 27 (1996) 71.
[17] R.K. Tyson, Principles of adaptive optics, Academic Press, San Diego, 1991.
[18] G.D. Love, J.V. Major, A. Purvis, Optics Lett. 19 (1994) 1170.
[19] R. Dou, M.K. Giles, Optics Lett. 20 (1995) 1583.
[20] G.D. Love, Appl. Optics 36 (1997) 1517.
[21] W. Klaus, N. Hashimoto, K. Kodate, T. Kamiya, Opt. Rev. 1 (1994) 7.
[22] K. Lu, B.E.A. Saleh, Opt. Eng. 29 (1990) 240.
[23] M. Born, E. Wolf, Principles of Optics, Pergamon Press, New York, 1980.
[24] W.J. Dallas, Appl. Optics 10 (1971) 673.
[25] E. Carcolé, J. Campos, I. Juvells, Optics Comm. 132 (1996) 35.
[26] I. Moreno, J. Campos, C. Gorecki, M.J. Yzuel, Jpn. J. Appl. Phys. 34 (1995) 6423.
[27] S. Mazé, P. Joffre, Ph. Réfrégier, Proc. Soc. Photo-Opt. Instrum. Eng. 1505 (1992) 20.
[28] J.C. Kirsch, D.A. Gregory, M.A. Thie, B.K. Jones, Opt. Eng. 31 (1992) 963.
[29] V. Laude, S. Mazé, P. Chavel, Ph. Réfrégier, Optics Comm. 103 (1993) 33.
[30] C. Soutar, S.E. Monroe, J. Knopp, Complex characterization of the Epson liquid crystal television, in: D.P. Casasent (Ed.), Optical Pattern Recognition IV, Proc. Soc. Photo-Opt. Instrum. Eng. 1959 (1993) 269.
[31] M. Yamauchi, T. Eiju, Optics Comm. 115 (1995) 19.
[32] Z. Zhang, G. Lu, F.T.S. Yu, Opt. Eng. 33 (1994) 3018.
[33] V. Laude, Optics Comm. 138 (1997) 394.
[34] I.S. Gradshteyn, I.M. Ryzhik, Table of Integrals, Series and Products, Academic Press, New York, 1980.
[35] E. Carcolé, S. Bosch, J. Campos, J. Mod. Optics 40 (1993) 1091.
[36] A. Yariv, P. Yeh, Optical Waves in Crystals, Wiley, New York, 1984.